COMPUTER SIMULATION OF EQUIAXED EUTECTIC SOLIDIFICATION OF METALS

A. Kermanpur, N. Varahraam and P. Davami

Department of Materials Engineering and Science
Sharif University of Technology,
P.O. Box 11365-9466, Tehran, Iran

(Received: Aug. 29, 1996 - Accepted in Revised form: April 8, 1999)

Abstract In the present work, the solidification process was simulated in both macroscopic and microscopic scales. Two-dimensional heat transfer equation for conduction was applied for macroscopic modelling using enthalpy formulation and finite element method. In order to decrease execution time and/or memory capacity in finite element analysis, skyline mathematical technique was adapted. The microenthalpy method using kinetic equations for microstructure formation was used for microscopic modelling. This macro-micromodelling is able to represent transient thermal field of the system, the enthalpy and solid fraction distributions, and different aspects of microstructure: grain density, size, eutectic interlamellar and dendrite arm spacings. A good agreement was found between our numerical data with some experimental results from several research sources.

Key Words Simulation, Solidification Process, Finite Element Method, Microstructure Formation, Eutectic Alloy

چکیده در کار حاضر فرآیند انجماد در دو مقیاس ماکروسکوپی و میکروسکوپی شبیه‌سازی شده است. برای الگوسازی ماکروسکوپی، معادله هدایت حرارت دو بعدی با استفاده از روش المان محدود و فرمولاسیون انتالپی حل شده است. به منظور کاهش زمان اجرا و حجم حافظه مورد نیاز در آنالیز المان محدود، روش ریاضی skyline مورد استفاده قرار گرفته است. الگوسازی میکروسکوپی نیز با بکارگیری معادلات سینتیک تشکیل ساختار میکروسکوپی و ادغام آنها در مدل انتقال حرارت براساس روش میکروانتالپی انجام شده است. مدل ماکرو-میکروسکوپی حاضر قادر به ارائه میدان حرارتی سیستم، توزیع انتالپی و کسر جامد به همراه جنبه‌های مختلف ریزساختاری نظیر اندازه و دانسیته دانه‌ها و فواصل بین لایه‌های یوتکتیکی و شاخه‌های دندریتی می‌باشد. نتایج حاصل از مدل عددی حاضر توافق خوبی را با نتایج تجربی گزارش شده در مراجع مختلف نشان می‌دهد.

INTRODUCTION

In recent years, heat transfer problems with phase change for solidification modelling has received much attentions. Due to the difficulties for the formulation of the above process, certain points should be taken into account throughly and analysed preciesely for a successfull modelling. These considerations are: the presence of transient phase change, media interfaces, different ways of 3-D heat transfers, and thermo-physical properties of different domains.

In spite of these difficulties, many attempts have been made in this direction in different ways: (1) macromodelling of heat transfer and fluid flow during mold filling and stress distribution accompaning solidification, and (2) micromodelling of solidification kinetics and fluid flow in the mushy zone. At macroscopic level, energy, mass, momentum and/or solute continuity equations have been used to calculate temperature field, mold filling, convection in the liquid, and macrosegregation. The early work in this field was by Murray and

Landis [1] in 1959. In this field, a simple model is considered for applying phase change in the equation system. However, this model can not predict the microstructural and metallurgical aspects of solidification. In 1966 Oldfield [2] applied the microstructural rules to the continuity equation of energy for microstructure evolution of gray cast iron. The goal of micromodelling of solidification is to obtain an appropriate solid fraction model that can be subsequently introduced into macroscopic heat flow calculations. This relates the solidification condition to undercoolings and to microstructural features [3]. However, due to the complexity of the process, it was not until 1984 that several research projects have been initiated in this field [3-12].

FORMULATION OF THE PRESENT ANALYSIS

In this work, the solidification of eutectic alloys was analysed in both macroscopic and microscopic levels.

"Macroscopic Model"

A. Governing Equation

In general, conservation equation of the energy represents the accumulation rate of the energy which is the result of conduction, convection or radiation of heat, heat generation of chemical reaction or phase change, fluid flow and/or the mechanical work as a result of phase change. Mathematical expression of this equation for a dependent variable ϕ is as follows:

$$\frac{\partial}{\partial \tau}\left[\rho\phi(r,\tau)\right] + \nabla.\left[\rho u(r,\tau).\phi(r,\tau)\right] = \nabla.\left[k(r,\tau)\nabla\phi(r,\tau)\right] \quad \dot{Q} \tag{1}$$

(Definition of the symbols is listed in the nomenclature).

Therefore, at macroscopic level, the solidification process of metals is controlled by heat diffusion and convection in the liquid [3,13]. The following assumptions were applied for present macroscopic model [14-16]:

(1)Solidification begins with initial uniform temperature distribution.

(2)Heat transfer is only by conduction.

(3)Heat transfer by conduction is considered in 2-D system.

(4)Thermo-physical properties in any medium is constant (see Table 1) and this domain is isotropic.

(5)No air gap formation exists in metal/mold interface.

At the present analysis, the enthalpy formulation was conducted and enthalpy function was defined as follows:

$$H(T) = \int_0^T C_p(T')dT' + L\left[1 - f_S(T)\right] \tag{2}$$

With the above mentioned assumptions, Equation 1 is converted to a cartesian two-dimensional space:

$$\rho t\frac{\partial H}{\partial \tau} = \frac{\partial}{\partial x}\left(kt\frac{\partial T}{\partial x}\right) + \frac{\partial}{\partial y}\left(kt\frac{\partial T}{\partial y}\right) \tag{3}$$

For solving Equation 3, we apply different initial and boundary conditions as follows:

$$T(r,0) = T_0(r) \quad , \quad r \in \Omega \tag{4}$$

$$T(r_i,\tau) = \hat{T}(r_i,\tau) \quad , \quad r_i \in \Gamma_1 \tag{5}$$

$$-k\frac{\partial T}{\partial n}(r_i,\tau) = q_{sB}(r_i,\tau) \quad , \quad r_i \in \Gamma_2 \tag{6}$$

$$-k\frac{\partial T}{\partial n}(r_i,\tau) = h_c(T(r_i,\tau) - T_{ac}) \quad , \quad r_i \in \Gamma_3 \tag{7}$$

$$-k\frac{\partial T}{\partial n}(r_i,\tau) = \bar{h}_r(r_i,T(\tau))\left[T(r_i,\tau) - T_{ar}\right] \quad , \quad r_i \in \Gamma_4 \tag{8}$$

where $\bar{h}_r$ is equivalent radiative heat transfer

coefficient and is given by:

$$\bar{h}_r(r_i,T(\tau)) = \varepsilon_B \sigma (T^2(r_i,\tau)+T_{ar}^2)(T(r_i,\tau)+T_{ar}) \quad (9)$$

The finite element method was used for solving Equaiton 3 [17].

B. Finite Element Model

For spatial discretization of the considered domain, three-node triangular elements were used and the governing differential equation was solved by Galerkin weighted residual method. The approximation of variables T and H over the element Ω^e was done by the following function:

$$T = \sum_{j=1}^{3} N_j^e(x,y).T_j^e(\tau) \quad (10)$$

$$H = \sum_{j=1}^{3} N_j^e(x,y).H_j^e(\tau) \quad (11)$$

Finally, the finite element model of Equation 3 is as follows:

$$\left[M^e\right].\left\{\dot{H}^e\right\} + \left[K^e\right].\left\{T^e\right\} = \left\{F^e\right\} \quad (12)$$

where $\left[M^e\right]$, $\left[K^e\right]$ and $\left\{F^e\right\}$ are mass and stiffness matrices and load vector, respectively. The form of the matrix elements and vectors are:

$$M_{ij} = \int_{\Omega^e} \rho N_i^e N_j^e \, tdxdy \quad (13)$$

$$K_{ij} = \int_{\Omega^e} k \left[\frac{\partial N_i^e}{\partial x}\frac{\partial N_j^e}{\partial x} + \frac{\partial N_i^e}{\partial y}\frac{\partial N_j^e}{\partial y}\right] tdxdy + \int_{\Gamma^e} \left[h_c N_i^e N_j^e + \varepsilon_B \sigma N_i^e (N_j^e.T^e)^3 N_j^e\right] td\Gamma \quad (14)$$

$$F_i^e = \int_{\Gamma_1^e} N_i^e(-q_{sB})td\Gamma + \int_{\Gamma_2^e} h_c N_i^e T_{ac} td\Gamma + \int_{\Gamma_3^e} \varepsilon_B \sigma N_i^e T_{ar}^4 td\Gamma \quad (15)$$

Applying constant temperature boundary condition (Dirichlet) in equation system is different from that of other boundary conditions (Neumman). The former is applied directly to equation system. For calculating M_{ij}^e, K_{ij}^e and F_i^e over each element, we need an appropriate integration method. In the case of simple shape and regular element, this integration can be done analytically. However, in the case of irregular elements, a numerical method as well as isoparametric transformation technique should be used.

The discretization of the time derivative in Equation 12 is most often achieved with a finite difference method. At the present work, we used one step θ-method for time stepping scheme. According to this method, the basic variable of equation system (i.e. enthalpy) is approximated as follows:

$$\langle H\rangle^{n+1} = \langle H\rangle^n + \Delta\tau\left[\theta\left\{\dot{H}\right\}^{n+1} + (1-\theta)\left\{\dot{H}\right\}^n\right] \quad (16)$$

where $0<\theta<1$ and label n on the variables indicates the time stage. For $\theta=0$, or explicit scheme, an unknown variable can be calculated directly. However, in order to secure the stability, time step should be small. For $\theta=1$, or implicit scheme, time step can be larger, but this method requires iterative solution scheme. For solidification problems, the implicit scheme as well as lumping of mass matrix is an appropriate method [18]. In this condition, the stability of the solution method is secured. This also prevents the oscillations in the temperature field in the neighbourhood of a freezing front. By applying the time steping scheme, we obtain:

$$\left[M^e\right]\left\{H^e\right\}^{n+1}+\theta\Delta\tau\left[K^e\right]\left\{T^e\right\}^{n+1}=\left[M^e\right]\left\{H^e\right\}^{n}-(1-\theta)\Delta\tau\left[K^e\right]\left\{T^e\right\}^{n}+\Delta\tau\left(\theta\left\{F^e\right\}^{n+1}+(1-\theta)\left\{F^e\right\}^{n}\right) \quad (17)$$

Here, since specific heat does not appear explicitly, the mass matrix is constant. However, for the stiffness matrix inconsistency as a result of presence of radiative boundary condition in the system, K and F should be recalculate at each time step. As can be seen in Equation 17, in the case of $\theta>0$, the presence of both enthalpy and temperature introduces a nonlinearity (because both are unknown). At the present work, for solving the nonlinear Equation 17, the Newton-Raphson method is used. By handling this method, we obtain:

$$\left\{\left[M^e\right]+\theta\Delta\tau\left[K^e\right]\left[\frac{\partial\left\{T^e\right\}}{\partial\left\{H^e\right\}}\right]_S^{n+1}\right\}.\{\Delta H\}=-\left[M^e\right]\left\{H^e\right\}_S^{n+1}-\theta\Delta\tau\left[K^e\right]\left\{T^e\right\}_S^{n+1}+\left[M^e\right]\left\{H^e\right\}^{n}-(1-\theta)\Delta\tau\left[K^e\right]\left\{T^e\right\}^{n}+\Delta\tau\left(\theta\left\{F^e\right\}_S^{n+1}+(1-\theta)\left\{F^e\right\}^{n}\right) \quad (18)$$

where:

$$\{\Delta H\}=\left\{H^e\right\}_{s+1}-\left\{H^e\right\}_s \quad (19)$$

Here, $\left[\partial\left\{T^e\right\}/\partial\left\{H^e\right\}\right]_S^{n+1}$ is called jacobian matrix in time τ_{n+1} and sth iteration (i.e. $[J]_S^{n+1}$). For reducing the required calculation time, $[J]^n$ can be used instead of $[J]_s^{n+1}$ (i.e. modified Newton-Raphson method). With $\theta=1$, Equation 18 becomes in symbolic form as follows:

$$\left\{\left[M^e\right]+\Delta\tau\left[K^e\right]\left[\frac{\partial\left\{T^e\right\}}{\partial\left\{H^e\right\}}\right]_S^{n+1}\right\}.\{\Delta H\}=-\left[M^e\right]\left[\left\{H^e\right\}_S^{n+1}-\left\{H^e\right\}^{n}\right]-\Delta\tau\left[K^e\right]\left\{T^e\right\}_S^{n+1}+\Delta\tau\left\{F^e\right\}_S^{n+1} \quad (20)$$

In the above equation, since all terms in time τ_n and τ_{n+1} with sth iteration are known, we can simply calculate $\left\{H^e\right\}_{s+1}$. For solving the resulting linear equation system, we use both inversion matrix and LU techniques.

All the above presented equations are valid for a typical element of the domain. So, for any mesh, the element equations are assembled and the boundary conditions are applied to them. In each time step, calculations continue iteratively until $\{\Delta H\}$ is smaller than a present error tolerance, $\in$. This criterion can be represented as a root-mean-square value of the normalized error in the global nodal values as follows:

$$\left[\frac{\{\Delta H\}^T.\{\Delta H\}}{\{H\}^T.\{H\}}\right]^{1/2}\le\varepsilon \quad (21)$$

where ε is a selected relative error.

In spite of high accuracy of the enthalpy method, the consuming time for calculations is relatively high. At the present analysis, in order to decrease the execution time of calculations, the resulting equation system was solved by skyline technique [17].

"Microscopic Model"

A. Introduction

In the present work, metallurgical equations of the microstructure formation for eutectic alloys were coupled with macroscopic enthalpy model using microenthalpy method [3]. The following assumptions have been considered:

(1) The continuous nucleation mechanism is taken into account.

(2) In any nuclei, once nucleated, the grain remains in fixed position, i.e., fluid flow and

convection are not considered.

(3) Grain growth continues to the end of solidification process, and coalescence and dissolution of existing grains are not considered.

(4) Grains are spherical and their shape remain unchanged during solidification until impingement.

(5) An average grain radius is used for calculations at each time step.

With these simplifications, one has to calculate real solid fraction of each element via an energy balance, which predicts correct temperature as well as microstructural aspects of the casting.

B. Nucleation Model

Considering many different sites present in liquid for nucleation and existence of undercoolings in these regions, a continuous nucleation model was considered. In this model, grain density is a function of cooling rate of which the value is calculated from instant undercooling. For this reason, a statistical model based on Gaussian distribution function was used [3] as follows:

$$\frac{dN(\triangle T)}{d(\triangle T)} = \frac{N_{max}}{\triangle T_\sigma \sqrt{2\pi}} .\exp\left[-\frac{(\triangle T-\triangle T_n)^2}{2(\triangle T_\sigma)^2}\right] \quad (22)$$

Therefore, at any undercooling $\triangle T(\tau_0)$, grain density can be calculated from:

$$N(\triangle T(\tau_0))=N_{min}+\frac{N_{max}}{\triangle T_\sigma \sqrt{2\pi}} \cdot \int_0^{\triangle T(\tau_0)} \exp\left[-\frac{(\triangle T-\triangle T_n)^2}{2(\triangle T_\sigma)^2}\right] d(\triangle T(\tau)) \quad (23)$$

where N_{max} , $\triangle T_n$, $\triangle T_\sigma$ should be presented for any alloy from the experiment and N_{max} is the minimum grain density of nuclei in the initial melt. The values used in the present analysis are presented in Table 2. This means that by using this model one can calculate the grain density for each element at any time τ .

C. Growth Model

In order to calculate the average grain size of each element, one has to use an appropriate growth model. For equiaxed growth mechanism of eutectic alloys, we can apply, with good approximation, the direct relationship between growth rate and square of the bulk undercooling (i.e. growth by screw dislocations) [3,19,20]. Therefore, we have;

$$\nu(\tau) = \frac{\beta(1+2g^{1/2})}{g} \cdot \frac{D_l L^2 (\triangle T(\tau))^2}{4\pi\sigma_{sl} T_m^3 k_B V_s} \quad (24)$$

or in a simpler form:

$$\nu(\tau) = \frac{dR(\tau)}{d\tau} = \mu.(\triangle T(\tau))^2 = \mu.\left[T_E - T(\tau)\right]^2 \quad (25)$$

where μ is the growth constant which should be calculated for any alloy. In the present work due to the lack of data, the value of μ for Al-12%Si alloy was calculated from previous data for cast iron using a computational method [21]. The computed value of μ is given in Table 2. Integration of Equation 25 gives the grain size in time τ_0 :

$$R(\tau_0)=R_{in}+\int_0^{\tau_0} \mu.\left[T_E-T(\tau)\right]^2 .d\tau \quad (26)$$

Assuming that solid fraction remains unchanged during nucleation stage, we can calculate the real average grain size:

$$\overline{N(\tau).R^3(\tau)} = N(\tau-\triangle\tau).\overline{R^3(\tau-\triangle\tau)} + \triangle N.R_{in}^3 \quad (27)$$

with assumptions:

$$\overline{R}=\frac{1}{N_{tot}}\sum_{i=1}^{N_{tot}}R=\left[\frac{1}{N_{tot}}\sum_{i=1}^{N_{tot}}R^2\right]^{1/2}=$$

$$\left[\frac{1}{N_{tot}}\sum_{i=1}^{N_{tot}}R^3\right]^{1/3}=R \qquad (28)$$

Therefore, in the present work, the grain density and the average grain size for evolution of microstructure were applied.

D. Heat Balance

If grain density and grain size are known from nucleation and growth models, the solid fraction at time τ can be calculated from:

$$f_S(\tau)=N(\tau).\frac{4}{3}\pi R^3(\tau).f_i(\tau) \qquad (29)$$

Although according to the above nucleation model the grain density is updated at each time step, its contribution, when deriving Equation 29 can be neglected. Therefore one has:

$$\frac{df_S(\tau)}{d\tau}=N(\tau).\left[4\pi R^2(\tau).f_i(\tau).\frac{dR(\tau)}{d\tau}+\frac{4}{3}\pi R^3(\tau).\frac{df_i(\tau)}{d\tau}\right] \qquad (30)$$

Substituting unity for internal solid fraction ($f_i(\tau)$) for eutectic alloy and using an appropriate grain impingement function (e.g. Johnson-Mehl approximation), the variation of solid fraction in this system can be calculated. Therefore a new and correct temperature is obtained:

$$Q_{ext}.\frac{S}{V}.\Delta\tau=\rho.\Delta H=\rho C_P.\Delta T-\rho L.\Delta f_S(\tau) \qquad (31)$$

Here, for the stability of microstructural calculations and for reducing computational time, we use a two time step procedure for calculations of microscopic model. This leads to a much finer time step, while remaining a fairly large time step for the macroscopic model.

COMPUTED RESULTS AND VALIDATION

A. Solidification of Al-12%Si Cylindrical Casting in the Sand Mold

Figure 1 shows the system used by Kanetkar et al. [12]. The selected area as well as boundary conditions are represented in Figure 2. The present analysis was done for this system, using macro time step and relative error of 0.1 (sec) and 0.01, respectively. At Figure 3, the simulated results are compared with the experimental ones for point (1) in Figure 2. Good agreement is seen between the experimental data, the simulation results, and the real path of solidification. For representation of the solidification sequence in case of departure from equilibrium, Figure 4 shows the enthalpy-temperature curves which correspond to the three points of the system. As can be seen, the deviation from the equilibrium curve (i.e. straight line) is quite evident, and this deviation is affected by the cooling rate.

B. Microstructural Results

In addition to the representation of the real path of solidification, micromodelling also enables us to predict many microstructural features. Here, the results of microstructural aspects for Al-12%Si cast bar were compared with those of other similar studies based on the cooling rate.

In Figure 5 the simulated results for maximum undercooling (ΔT_{max}) are compared with those obtained from the experimental work

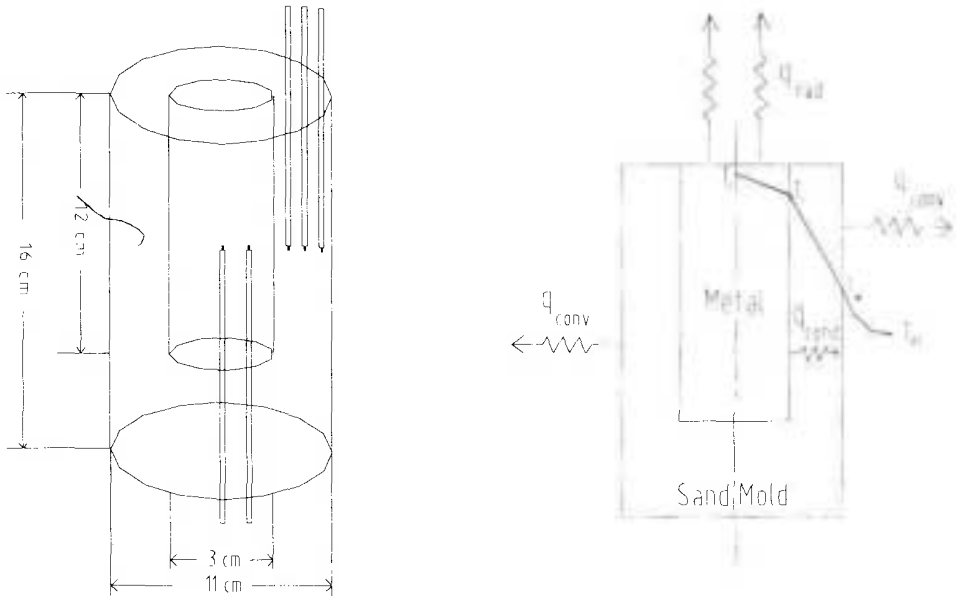

(a) (b)

Figure 1. Configuration of the casting and the mold geometries as well as boundary conditions.

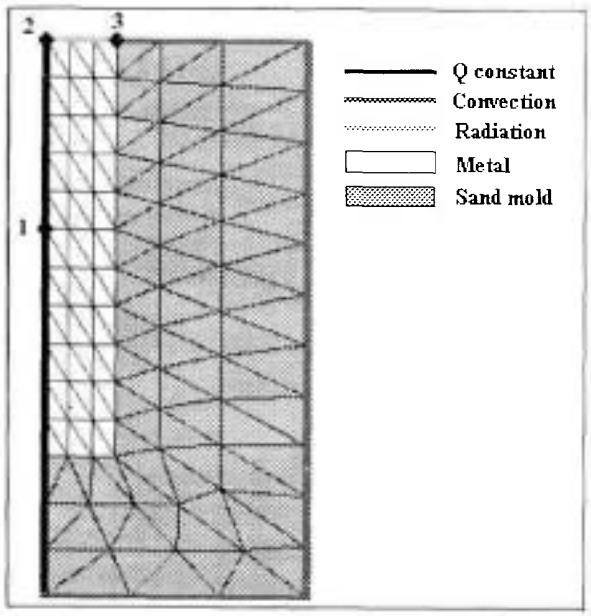

Figure 2. Two-dimensional finite element mesh of the system.

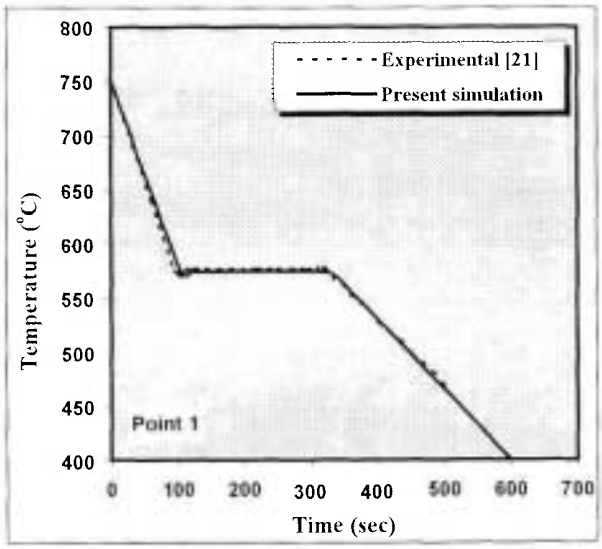

Figure 3. Comparison of the simulated and experimentally determined cooling curves at point (1) in Figure 2.

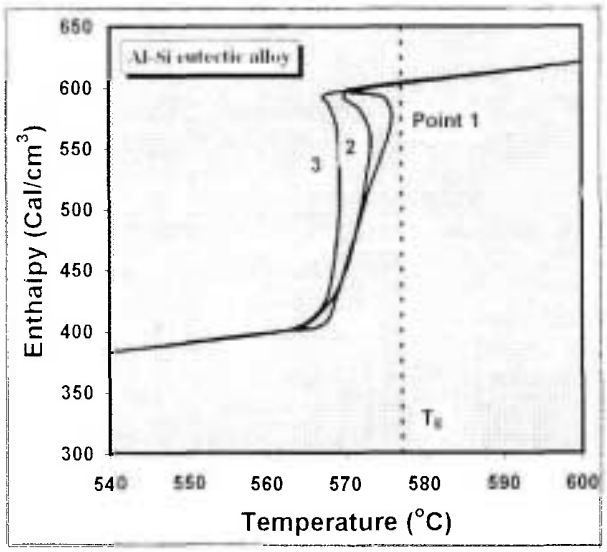

Figure 4. Simulated curves of enthalpy versus temperature for three points in Figure 2.

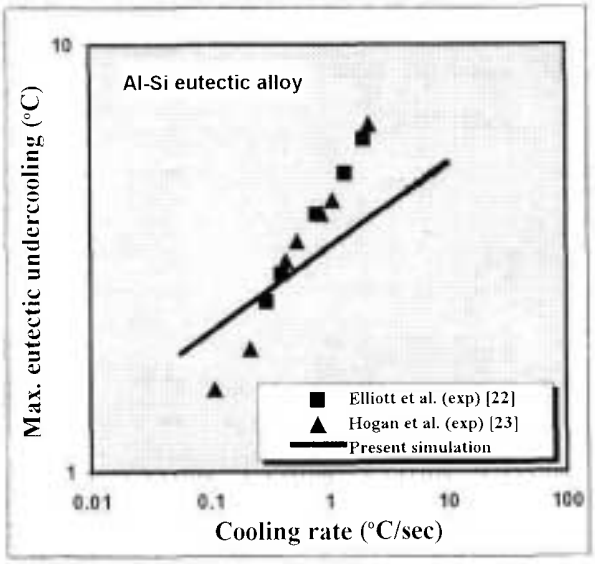

Figure 5. Comparisons of the simulated and experimentally determined maximum eutectic undercooling for Al-12%Si alloy.

of Elliott et al. [22] and Hogan et al. [23]. The maximum undercooling represented is the temperature difference between the eutectic temperature and the local minimum value in the cooling curve near to recalescence. In Figure 6,

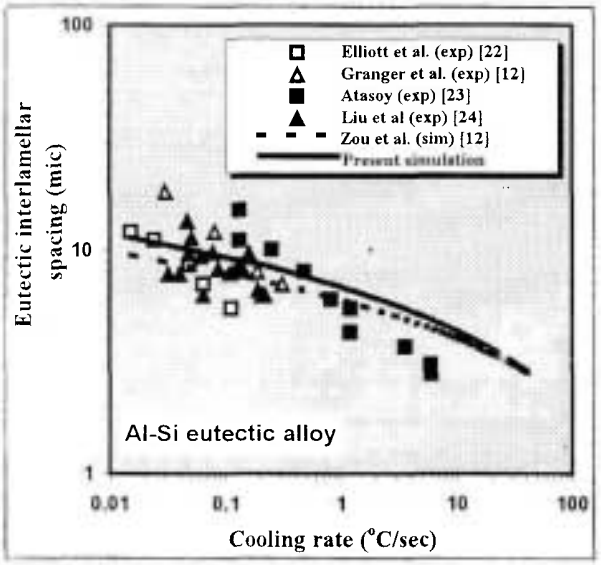

Figure 6. Comparisons of the simulated and experimentally determined eutectic interlamellar spacing for Al-12%Si alloy.

the simulated results of eutectic interlamellar spacing are compared with experimental results of Elliott et al. [22], Granger et al. [12], Atasoy [23], and Liu et al. [12]. As can be seen, although the experimental data are dispersed, the trend of simulated results are in good agreement with them. Calculations for eutectic interlamellar spacing was based on the following equation:

$$\lambda(\tau).\left[\nu(\tau)\right]^{a}=b \qquad (32)$$

where for Al-Si eutectic alloy, a and b are 0.457 and 0.337, respectively. This eutectic interlamellar spacing is an average value since this is a time dependent variable. The average spacing was calculated by dividing the total area under a given curve by the total elapsed time. Secondary dendrite arm spacing (SDAS) is evaluated approximately by the following equation:

$$\mathrm{SDAS}=5.5(\mathrm{M}.\tau_{\mathrm{f}})^{1/3} \qquad (33)$$

where M is the coarsening factor. Since in Al-Si

eutectic alloy, the α-phase grows dendriticly [25], dendrite arm spacing is analysed for this alloy. In Figure 7, the simulated results of secondary dendrite arm spacing are compared with experimental results of Tamminen [12], AFS atlas [25] and calculated results of Zou et al. [12]. Clearly, SDAS is proportional to local solidification time (τ_f) . It is seen that the present simulated results compare approximately well with those of experimental values as well as other simulated ones. One of the reasons for the discrepancies appeared in Figure 7 is that the coarsening factor (M) used in Zou's analysis had been for A356 alloy, whereas the present simulation focuses on Al-Si eutectic alloy.

In the present work, a post-processing module was developed for graphic presentation of the simulation results. As an example, the map of calculated grain size within the casting is shown in Figure 8.

CONCLUSIONS

Macro-microscopic simulation of solidification

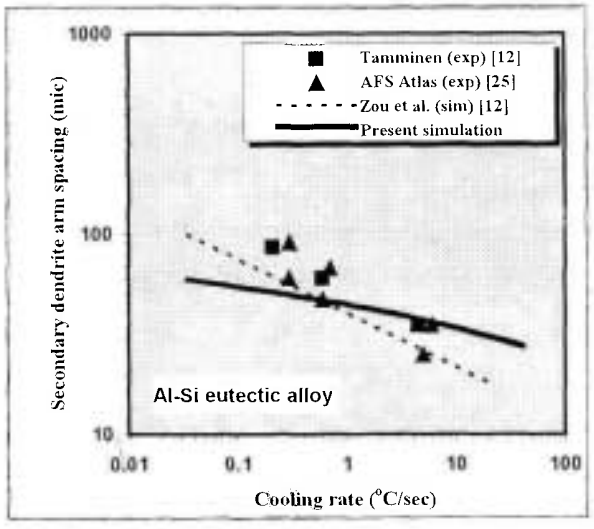

Figure 7. Comparisons of the simulated and experimentally determined secondary dendrite arm spacing for Al-12%Si alloy.

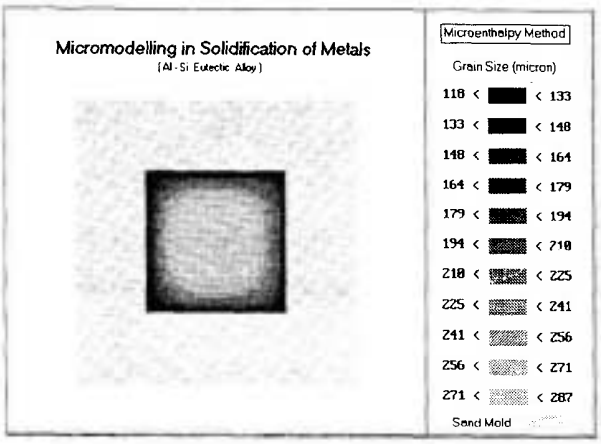

Figure 8. Map of simulated grain size for Al-12%Si alloy.

for eutectic alloys is proposed. At the macroscopic scale, the heat diffusion equation was solved using finite element method. Skyline technique was adapted for speed up the calculation. At the microscopic scale, the microenthalpy method was used for microstructure evolution. This macro-micromodelling enables us to represent real path of solidification as well as microstructural features of the casting. However, for a full and correct representation of microstructure characteristics, it is desired to invoke a robust method for solving the kinetic governing equations as well as considerations of the equiaxed/columnar transition in the system.

ACKNOWLEDGMENTS

The authors would like to gratefully acknowledge for assistance and helpful discussion of solidification simulation group in department of materials science and engineering, and financial support of vice-chancellor of research, Dr. M. Kermanshah, Sharif University of Technology, Tehran, Iran.

TABLE 1. Thermo-physical Properties of Al-12%Si Alloy [21]

k (cal/gr.sec.°C)	ρ (gr/cm^3)	C_P (cal/gr.°C)	L (cal/gr)	T_E (°C)	T_0 (°C)
0.2225	2.000	0.3544	96.89	577.0	750.0

TABLE 2. Various Parameters Used in the Microscopic Model [3,10,21].

N_{min} (cm^{-3})	N_{max} (cm^{-3})	ΔT_n (°C)	ΔT_σ (°C)	μ (cm/sec/(°C)^2)	R_{in} (mic)	M (cm^3/sec)
0	10000	10.0	4.0	5.38×10^{-5}	0.01	6.011×10^{-12}

NOMENCLATURE

C_p Specific heat
D_i Solute diffusion coefficient in liquid
f_i Internal solid fraction
f_s Solid fraction
F_i Coefficients in the finite element formulation (Equation 15)
g Diffuseness parameter
h Convective heat transfer coefficient
h_r Radiative heat transfer coefficient
H Specific enthalpy
H_j^e Enthalpy at the jth node of the element Ω^e
k Thermal conductivity
k_B Boltzmann constant
K_{ij} Coefficients in the finite element formulation (Equation 14)
L Latent heat of solidification
M Coarsening factor
M_{ij} Coefficients in the finite element formulation (Equation 13)
n Unit normal on the boundary
N Number of nuclei per unit volume (grain density)
N_i^e Interpolation function associated with ith node of element Ω^e
N_j^e Lagrange interpolation function of the element Ω^e
N_{max} Maximum grain density
N_{min} Minimum grain density
N_{tot} Total (final) grain density
q_{cB} Heat flux from convection
q_{rB} Heat flux from radiation
q_{iB} Imposed heat flux
Q Heat generation rate per unit volume
Q_{ext} External heat flux
r Position vector
R Radius of the growing nuclei at time τ
R Average grain radius
R_{in} Initial radius of nuclei
S Surface of the element
SDAS Secondary dendrite arm spacing
t Thickness of the domain
T Temperature
T Constant temperature
T_o Pouring temperature
T_{ac} Temperature for which no convection occured
T_{ar} Temperature for which no radiation occured
T_E Eutectic temperature

T_j^e	Temperature at the jth node of the element Ω^e
T_m	Melting point of the pure metal
u	Velocity vector
v	Growth rate of equiaxed eutectic grain
V	Volume of the element
V_s	Molar volume of the clusters
x,y	Cartesian co-ordinates

Greek Symbols

β	Correction factor (Equation 24)
Γ	Total boundary of Ω
Γ^e	Boundary of element Ω^e
$\triangle H$	Enthalpy increment
$\triangle T$	Undercooling
$\triangle T_n$	Mean nucleation undercooling corresponding to the maximum of the distribution
$\triangle T_\sigma$	Standard deviation of the distribution
$\triangle\tau$	Time increment
$\in$	Error tolerance for convergence
$\in_B$	Emissivity coefficient
θ	Parameter in the time approximation
λ	Eutectic interlamellar spacing
μ	Growth rate constant
ρ	Density
σ	Stefan-Boltzmann constant
σ_{sl}	Surface energy of solid/liquid interface
τ	Time
τ_f	Local solidification time
Ω	Total domain of the problem
Ω^e	Element domain

REFERENCES

1. W.D. Murray and F. Landis, "Numerical and Machine Solutions of Transient Heat Conduction Problems Involving Melting and Freezing -I. Method of Analysis and Machine Solutions", ***Trans. ASME, J. of Heat Transfer***, (May 1959), 106-112.
2. W. Oldfield, "A Quantitative Approach to Casting Solidification: Freezing of Cast Iron", ***ASM Trans.***, (1966), 59, 954-961.
3. M. Rappaz, "Modelling of Microstructure Formation in Solidification Processes", ***Int. Mat. Rev.***, (1989), 34(3), 93-123.
4. Ph. Thevoz et al., "Modelling of Equiaxed Microstructure Formation in Casting", ***Met. Trans. A***, (1989), 20(2), 311-322.
5. M. Rappaz and D. M. Stefanescu, "Modelling of Microstructural Evolution", ***Metals Handbook***, Casting, 9th. ed., ASM, (1988), 883-391.
6. E. Fras et al., "Macro and Micro Modelling of the Solidification Kinetics of Castings", ***AFS Trans.***, (1992), Paper 48.
7. D. M. Stefanescu and C. Kanetkar, "Computer Modelling of the Solidification of Eutectic Alloys: The Case of Cast Iron", in ***Computer Simulation of Microstructural Evolution***, D. J. Srolovitz ed., TMS-AIME, (1986), 171-188.
8. I. Minkoff, "How do Cast Iron Solidify? A Review of Micromodelling Using the Computer, Supporting Experiments and Basic Theory", ***The Found. J.***, (Jan/Feb 1993), 16-22.
9. D. M. Stefanescu et al., "Heat Transfer-Solidification Kinetics Modelling of Solidification of Castings", ***Met. Tarns. A***, (1990), 21A, 997-1005.
10. M. Rappaz and D. M. Stefanescu, "Modelling of Equiaxed Primary and Eutectic Solidifiaction", in ***Solidification Processing of Eutectics***, D. M. Stefanescu et al., TMS, Warrendale, PA, (1988), 133-151.
11. S. Chang et al., "Modelling of the Liquid/Solid and the Eutectic Phase Transformation in Spheroidal Graphite Cast Iron", ***Met. Trans. A***, 23, (1992), 1333-1346.
12. J. Zou et al., "Modelling of Microstructure Evolution and Microporosity Formation in Cast Aluminum Alloys", ***AFS Trans.***, (1990), Paper 178, 871-878.
13. M. Salcudean and Z. Abdullah, "On the Numerical Modelling of Heat Transfer During Solidification Processes", ***Int. J. for Num. Meth. in Eng.***, (1988), 25, 455-473.
14. A. Kermanpur, M.Sc. Thesis no. M40, Department of Metallurgical Engineering, Sharif University of Technology, Tehran, Iran, (October 1994).
15. A. Kermanpur et al., "Application of Finite Element Analysis in Solidification Simulation of Castings using Enthalpy Method", ***6th Annual Iranian Foundrymen's***

Society Seminar, (16-18 May 1994), Iran University of Science and Technology, Tehran, Iran.

16. A. Kermanpur and P. Davami, "Macroscopic Simulation of Solidification Process of Metallic Materials using Finite Element Analysis", ***3rd Annual Mechanical Engineering Society Conference***, (15-17 May 1995), Amir Kabir University of Technology, Tehran, Iran.
17. F. Stasa, "Applied Finite Element Analysis for Engineering", CBS Pub., Japan, (1985).
18. A. J. Dalhuijsen and A. Segal, "Comparison of Finite Element Techniques for Solidification Problems", ***Int. J. for Num. Meth. in Eng.***, (1986), 23, 1807-1829.
19. M. C. Flemings, "Solidification Processing", McGraw-Hill, New York, (1974).
20. D. M. Stefanescu and C. Kanetkar, "Computer Modelling of the Solidification of Eutectic Alloys: Comparison of Various Models for Eutectic Growth of Cast Iron", ***State of the Art of Computer Simulation of Casting and Solidification Processes***, H. Fredriksson ed., E-MRS, Strasbourg, France, (1986), 255-266.
21. C. S. Kanetkar et al., "A Latent Heat Method for Macro-Micro Modelling of Eutectic Solidification", ***Trans. ISIJ***, (1988), 29, 860-868.
22. R. Elliot and S.M.D. Glenister, "The Growth Temperature and Interflake Spacing in Aluminum Silicon Eutectic Alloys", ***Acta Metall.***, (1980), 28, 1489.
23. L.M. Hogan and H. Song, "Interparticle Spacings and Undercoolings in Al-Si Eutectic Microstructures", ***Met. Trans. A***, (1987), 18, 707-713.
24. J. Liu et al., "Lamellar Eutectic Stable Growth-I, II: Modelling & Experiment on Al-Si Eutectic", ***Acta Metall.***, (1990), 38, 1625-1634.
25. "Solidification Characteristics of Aluminum Alloys", American Foundrymen's Society, Volume: Foundry Alloys, (1991).